JOURNAL OF COMPUTATIONAL PHYSICS 82, 429–453 (1989)

The Spatially Non-uniform Convergence of the Numerical Solutions of Flows*

ARGYRIS G. PANARAS

Agias Elenis 63, Athens 15772, Greece

Received November 18, 1987; revised July 18, 1988

The spatial distribution of the numerical disturbances that are generated during a numerical solution of a flow is examined. It is shown that the distribution of the disturbances is not uniform. In regions where the structure of a flow is simple, the magnitude of the generated disturbances is small and their decay is fast. However in complex-flow regions, as in separation and vortical areas, large-magnitude disturbances appear and their decay may be very slow. The observed nonuniformity of the numerical disturbances makes possible the reduction of the calculation time by application of, what may be called, the partial-grid calculation technique, in which a major part of the calculation procedure is applied in selective subregions, where the velocity disturbances are large, and not within the whole grid. This technique is expected to prove beneficial in large-scale calculations such as the flow about complete aircraft configurations at high angle of attack. Also, it has been shown that if the Navier–Stokes equations are written in a generalized coordinate system, then in regions in which the grid is fine, such as near solid boundaries, the norms become infinitesimally small, because in these regions the Jacobian has very large values. Thus, the norms, unless they are unscaled by the Jacobian, reflect only the changes that happen at the outer boundaries of the computation domain, where the value of the Jacobian approaches unity and not in the whole flow field.

1. INTRODUCTION

For the numerical calculation of a flow, a reasonable initial solution is selected and an iterative process is applied until, by means of one or more convergence criteria, a converged solution is reached. The iterative procedure may last a few steps, or hundreds, or even thousands of steps, depending mainly on the nature of the flow, but also on the fineness of the grid and on the type of the numerical scheme.

The convergence criteria that are currently used are numerical or physical ones. Thus, during a numerical solution, one may observe the variation of one of the norms of the residual of the finite-difference equations, or the variation of the difference of the calculated quantities, from step to step, or, if appropriate, one may

* Work done while the author held a National Research Council/NASA Ames Research Center Research Associateship.

0021-9991/89 $3.00

check the value of a physical quantity, such as the lift or the pressure coefficient. In the first case, the calculation terminates when the norms or the differences reach an assumed "zero" value, while, in the latter case, when no more change is observed in the value of the coefficient.

The classical convergence criteria reflect the variation of the mean value of a quantity and they do not give information about the distribution of this quantity within the examined flow field. However, the flows in general are nonuniform. Especially large nonuniformities are observed in separated and vortex flows, in flows near boundaries, in shear flows, and in shock waves. In all these cases the kinematic and, probably, the thermodynamic quantities are subjected to a large variation, often in a region that is just a small portion of the whole flow field. Therefore it is expected that during the development of a numerical solution more steps will be required for the decay of the disturbances in these "complex" flow-regions, rather than in the ones which have a simpler structure.

In this paper it will be shown that indeed, the intensity of the generated disturbances to the calculated flow quantities and the time required for their decay is much higher in the complex-flow regions than in the simple-structure regions. Also, it will be shown that instead of the standard repetition of the numerical integration across all the extent of the computational domain (grid), until the solution converges, it is possible to do a part of the calculation cycle selectively, in subregions characterized by large values of the disturbance field. In this case the overall time required for the calculation of a flow will be smaller. Considering the present requirements for large-scale calculations about bodies at high incidence, this possibility is attractive. That because these types of flows are characterized by a rather simple structure in the windward side, and by a complex structure in the leeward side. Also, the computer time required for the estimation of the flow field about a modern air vehicle is of the order of tens of hours in a supercomputer. Thus there is a need to reduce the required computer time.

For the calculation of the flows which are used for the study of the numerical disturbance fields, the code F3D of NASA Ames [1] was used. The code F3D is a two-factor, implicit, approximately factored, finite-difference code which solves a conservative form of the thin-layer Navier–Stokes equations cast in generalized coordinates, so that it can be readily used for computing flows about complex configurations.

In the generalized form, all the terms of the Navier–Stokes equations are divided by the transformation Jacobian of the coordinates: $J = \partial(\xi, \zeta, \eta)/\partial(x, y, z)$. The value of the Jacobian within a grid may vary by orders of magnitude. Especially large values are observed near walls, where usually the grid is fine, while at the outer layers of a grid the Jacobian tends to unity. It will be shown that this variation may have a significant masking effect on the numerical mean-value convergence criteria, if the various quantities on which these criteria are based are not unscaled by the Jacobian. By combining the mean-value convergence criteria with surveys of the disturbance fields it was found that, unless the criteria are unscaled, the level of the disturbances near the wall is not shown.

2. Governing Equations and Calculations Procedures

The conservation equations of mass, momentum, and energy can be represented in a flux-vector form that is convenient for numerical simulation as [1]:

$$\partial_\tau \hat{Q} + \partial_\xi(\hat{F} + \hat{F}_v) + \partial_\eta(\hat{G} + \hat{G}_v) + \partial_\zeta(\hat{H} + \hat{H}_v) = 0, \tag{1}$$

where τ is the time, and the independent spatial variables ξ, η, and ζ are chosen to map a curvilinear, body-conforming discretization into a uniform computational space. In the system used in this study, ξ denotes the curvilinear axis in the direction of the main body axis, η denotes the circumferential, and ζ the normal to the body direction. As opposed to the inviscid flux terms $\hat{F}$, $\hat{G}$, and $\hat{H}$, the terms $\hat{F}_v$, $\hat{G}_v$ and $\hat{H}_v$ are fluxes containing the viscous derivatives. A nondimensional form of the equations is used throughout this work. Lengths are scaled by the length of the body, L, velocity components by the free-stream velocity of sound, a_∞, the pressure and the total energy per unit volume (e) by $\rho_\infty a_\infty^2$. The other quantities, such as T, ρ, μ are scaled by their free-stream values.

For body-conforming coordinates and high Reynolds number flow the thin-layer approximation can be applied [2, 3, 4],

$$\partial_\tau \hat{Q} + \partial_\xi \hat{F} + \partial_\eta \hat{G} + \partial_\zeta \hat{H} = \mathrm{Re}^{-1}\, \partial_\zeta \hat{S}, \tag{2}$$

where only viscous terms in the normal to the body direction are retained. These have been collected into the vector $\hat{S}$ and the nondimensional Reynolds number Re is factored from the viscous flux term.

An implicit approximately factored scheme for the thin-layer, Navier–Stokes equations that uses central differencing in the η and ζ directions and upwind differencing in the ξ direction can be written in the form

$$\begin{aligned}
&[I + h\delta_\xi^b(\hat{A}^+)^n + h\delta_\zeta \hat{C}^n - h\,\mathrm{Re}^{-1}\,\delta_\zeta J^{-1}\hat{M}^n J - D_i|_\zeta] \\
&\quad \times [I + h\delta_\xi^f(\hat{A}^-)^n + h\delta_\eta \hat{B}^n - D_i|_\eta]\, \Delta\hat{Q}^n \\
&= -\Delta t\{\delta_\xi^b[(\hat{F}^+)^n - \hat{F}_\infty^+] + \delta_\xi^f[(\hat{F}^-)^n - \hat{F}_\infty^-] \\
&\quad + \delta_\eta(\hat{G}^n - \hat{G}_\infty) + \delta_\zeta(\hat{H}^n - \hat{H}_\infty) - \mathrm{Re}^{-1}\,\delta_\zeta(\hat{S}^n - \hat{S}_\infty) \\
&\quad - D_e(\hat{Q}^n - \hat{Q}_\infty)\},
\end{aligned} \tag{3}$$

where $h = \Delta t$ or $\Delta t/2$ for first- or second-order time accuracy, and the free-stream base solution is used. Here δ is typically a three-point, second-order accurate, central difference operator, δ is a midpoint operator used with the viscous terms, and the operators δ_ξ^b and δ_ξ^f are backward and forward three-point difference operators. The flux $\hat{F}$ has been split into $\hat{F}^+$ and $\hat{F}^-$, according to its eigenvalues [5], and the matrices $\hat{A}^\pm$, $\hat{B}$, $\hat{C}$, and $\hat{M}$ result from local linearization of the fluxes about the previous time level. In Eq. (3), J denotes the Jacobian of the coordinate transforma-

tion. Dissipation operators, D_e and D_i, are used in the central space differencing directions [1].

The factored left-hand side operators can be readily solved by sweeping in the ξ direction and inverting tridiagonal matrices with five by five blocks. This two-factor implicit scheme is readily vectorized in planes of $\xi = \text{constant}$.

Concerning the calculation procedure, during a numerical solution of a flow, it is known that in case of unsteady flows a time-accurate method must be employed. After the selection of some reasonable initial solution, an integration in time is done, with time steps commensurate with the unsteady phenomenon that is calculated. In steady state calculations, usually non-time-accurate techniques are applied, which bring the flow from an arbitrary initial gues to its asymptotic solution, with the least possible computational work. The use of a space varying time step is a classical technique, in this sense.

Often, for simplicity, the impulsive start, i.e., the sudden immersion of a body in a uniform flow, is used. Various techniques have been developed that accelerate the convergence. For both steady and unsteady flows, a faster convergence is reached if instead of the impulsive start, a solution of a similar flow is applied initially. Also, in the case of an unsteady flow, it is better to calculate first an approximate steady solution and then to apply the time-accurate calculation. One way to accelerate convergence to a steady state is to obtain a good initial guess for a fine mesh by first iterating on a sequence of coarse grids and then interpolate the solution up to the next refined grid (see, for example, [6]). This is called the "nested iteration" procedure and basically originates from the well-known multigrid method.

Some of the described techniques of acceleration of the convergence will be applied in the numerical solution of the flows that are used in this work, for studying their effect in the numerical disturbance field.

3. Description of the Calculated Flows

In this section, the flows that have been used for studying the spatial variation of the disturbance field will be briefly described. The detailed results of the investigated flows will be reported in other particular publications.

The first case is related to the calculation of the turbulent flow about a prolate spheroid, at $\alpha = 30°$, $M_\infty = 0.25$ and $\text{Re}_l = 43 \times 10^6$. The prolate spheroid is a body of simple geometry that can provide significant understanding of the complex flow that can develop about axisymmetric bodies at incidence. In a cross section of such a flow, under the action of circumferential pressure gradient, the outer flow approaching the windward plane of symmetry turns and flows outwards along the body, from the windward toward the leeward side. The boundary layer which is formed in this way, separates from the body at a point on the leeward side. The fluid then leaves the body along a feeding sheet and rolls up to form a primary vortex system on the leeward side of the body. The pair of the primary vortices induces a flow toward the body surface, which at the point of attachment turns

outwards toward the windward side. For primary vortices of sufficient strength, a secondary separation is induced to the boundary layer below them. Thus, a secondary vortex structure may appear that rotates in an opposite direction from the primary one. Both the vortex systems are carried downstream by the axial component of the flow.

Results of the calculations are shown in Fig. 1. The primary vortex structure is clearly shown in the velocity–vectors plot (Fig. 1b), while the existence of the secondary vortex is detected more easily in Fig. 1a, where surface particle traces are used to simulate the surface shear stress lines visualized in oil flow experiments. These lines converge toward the primary and the secondary separation lines and diverge from the attachment line, which lies between them.

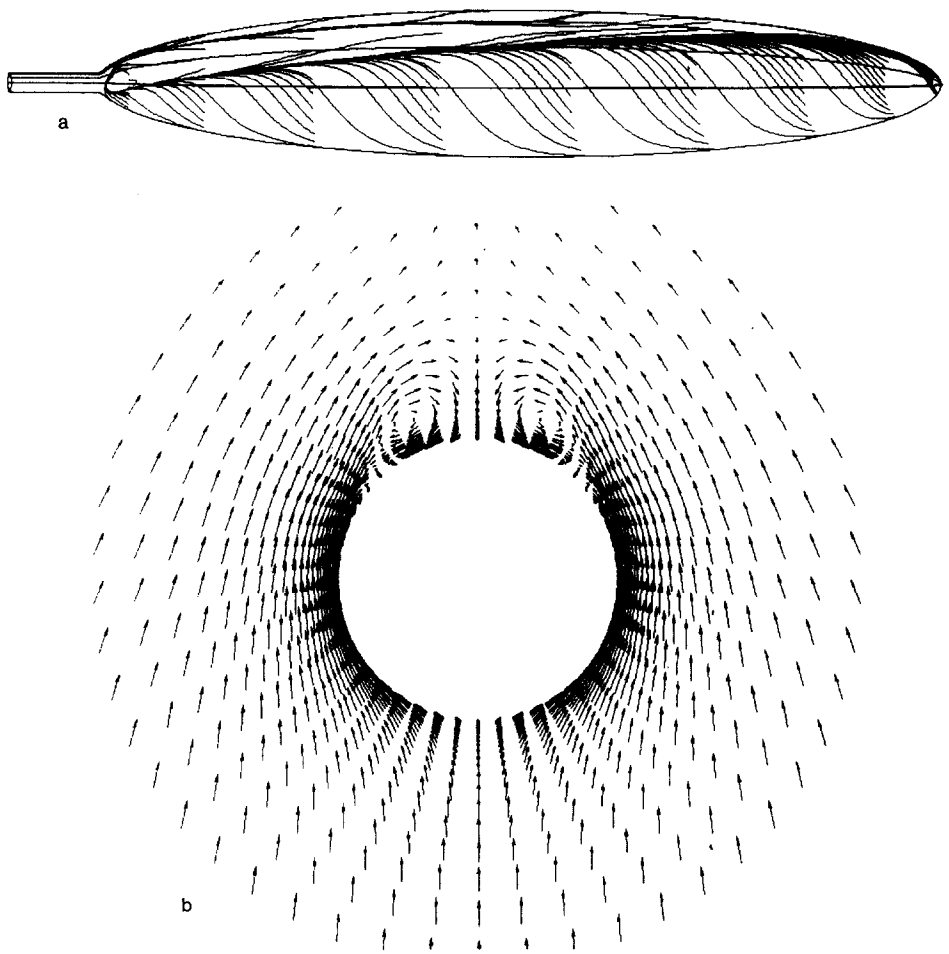

FIG. 1. The calculated flow field about the prolate spheroid: (a) surface oil flow simulation; (b) crossflow velocity vectors at $x/L = 0.50$.

The calculation was non-time-accurate, with the time step varying in space, as a function of the local Jacobian. No similar solution was available, so the flow was started by imposing impulsive conditions. The grid that was used consisted of 121 points along the direction of the main axis of the body, 100 points around its circular section and 65 points radially from the surface. Initially, for accelerating the solution, a coarse grid was used. That grid was formed by considering each second point of the regular grid, in the streamwise and in the circumferential directions. Also, the values of the coefficients of the numerical viscosity terms of Eq. (3), initially were rather large, also for the purpose of acceleration of the convergence.

A final change that was imposed during the numerical solution was related to an improvement of the turbulence model. The standard model used in the code F3D, is the two-layer, Cebeci type, algebraic eddy-viscosity model reported by Baldwin and Lomax (Ref. [2]). In this model the value of the turbulence viscosity coefficient, μ_t, at a particular velocity profile is a function of the maximum of the product of the vorticity and the distance from the wall. Degani and Schiff [7] have observed that in flows which include crossflow vortices there exist two maxima in the distribution of the vorticity product in the velocity profiles, one caused by the boundary layer and one caused by the overlying vortical structure. The consideration of only the lower maximum gives better results. In the calculation of the flow about the prolate spheroid, initially no distinction had been made between the maximum of the vorticity product caused by the boundary layer and the one caused by the vortex. Later in the calculation, this distinction was considered. This change affected strongly the separated vortical region. The primary vortices became larger and the secondary vortices, which previously had not shown, appeared. The attached-flow was not affected by this change because there the value of the μ_t was kept the same.

All of the forementioned changes that were applied during the calculation had an impact in the state of the numerical solution, in the sense that when one of these changes was imposed, the solution was perturbed. Thus, an excellent opportunity appeared for studying the spatial growth and decay of the velocity perturbations during the process of convergence.

The second case that is used in this work is related to the impingement of a jet, in the presence of a crossflow. In the simulation, the jet was originated from a nozzle and it was directed perpendicularly to the ground. The ratio of the crossflow velocity to the mean jet velocity was equal to 0.223, and the Reynolds number, based on the diameter of the nozzle, was 4.4×10^5. The flow was calculated as a turbulent one. Van Dalsem [8] has investigated the case where the nozzle has a circular cross section. The present author has studied the case of a jet of elliptical cross section [9]. The axes ratio has been variable and the major axis has been aligned or normal to the crossflow. In this paper, the case of axes ratio equal to 1.5, with the major axis aligned with the crossflow, will be used for the study of the numerical disturbance field.

In this case the calculations were time accurate and the solution of the round jet was used as the initial one. After changing the grid to account for the new cross sec-

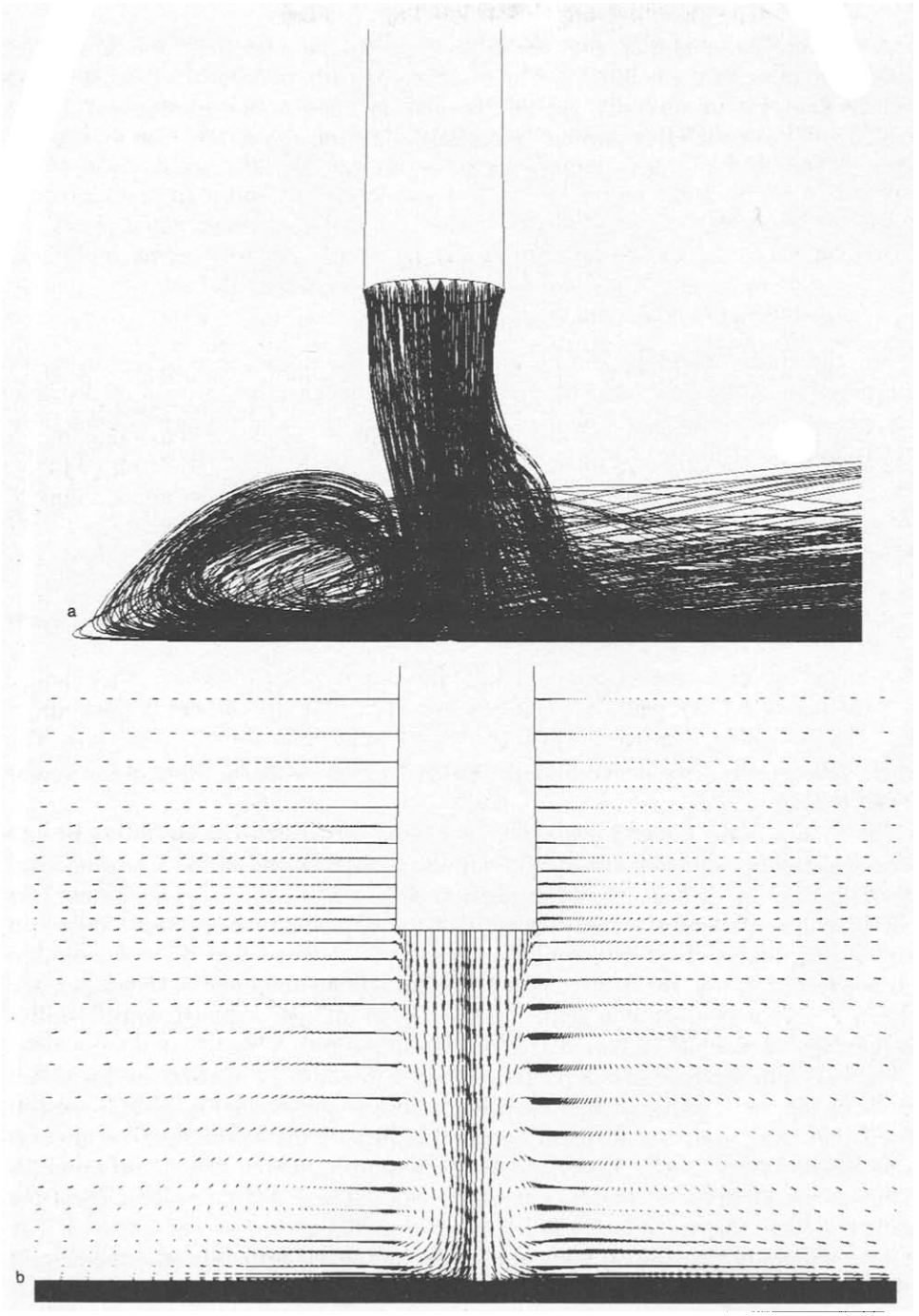

FIG. 2. Results of jet in crossflow: (a) trajectories of particles released from the jet; (b) velocity vectors in the streamwise symmetry plane.

tion, the calculation started with the assumption that at each point the flow quantities were those of the round jet. The resulting perturbation and its gradual decay will be analysed in the next section. To give an idea of the particular flow, in Fig. 2a, the trajectories of particle traces released from the nozzle face are shown. Also, in Fig. 2b the velocity vectors are shown in the vertical symmetry plane.

4. Results

4.1. *Generation and Decay of the Disturbances*

For the study of the generation and decay of the disturbance field during the computation of the flows that have been selected, mean-value, as well as distribution convergence criteria will be used. The l_2 norm, or Euclidean norm, is the most widely used mean-value criterion. It reflects the change of the residual of the finite-difference equations. In this paper, the l_2 norm will be used, scaled or unscaled, with the Jacobian. In addition, the mean-value of ΔQ will be used. Refering to Eq. (3) and a grid of N points, these quantities are defined by:

$$l_2 \text{ norm} = \sqrt{\frac{1}{N} \sum_{i=1}^{N} \sum_{j=1}^{5} R^2(\mathbf{r}_i, j)} \tag{4}$$

$$\Delta Q = \sqrt{\frac{1}{N} \sum_{i=1}^{N} \sum_{j=1}^{5} \{\Delta Q^n(\mathbf{r}_i, j)\}^2} \tag{5}$$

where $R(\mathbf{r}_i, j)$ denotes the 5-component RHS of Eq. (3), $\mathbf{r}_i$ being the position vector of the various grid points.

The change of the velocity field (Δu_i, $i = 1, 2, 3$) between two successive steps, has been selected for studying the spatial variation of the disturbance of a numerical solution. The Δu_i is defined by the relation $u_i^{n+1} = u_i^n + \Delta u_i$. In what follows, Δu_i will be called the velocity disturbance. When the velocity disturbance during a numerical solution of a flow is equal to zero, it is assumed that the flow solution has converged. In the various velocity plots that will be presented in this paper, the Δu_i have been magnified by a factor of 10^3–10^5, so that their change will be visible. In this type of plot the vectors may cross a solid boundary.

Starting with the case of the prolate spheroid, the history of the generation and decay of the mean value of the ΔQ-disturbances is shown in Fig. 3. It is seen in Fig. 3 that the initial strong perturbation, because of the assumption of uniform flow conditions gradually decays, but not smoothly. Three large discontinuous increases are observed in the velocity disturbance. These discontinuities reflect the perturbation of the numerical solution each time that a change was imposed. The first discontinuity appears at $N = 250$ (number of iterations), where the coarse-grid solution was interpolated into the fine grid. The next change was imposed at $N = 530$, and it was related to the reduction of the values of the coefficients of the numerical dissipation terms. Again, this disturbance has shown up in the ΔQ curve,

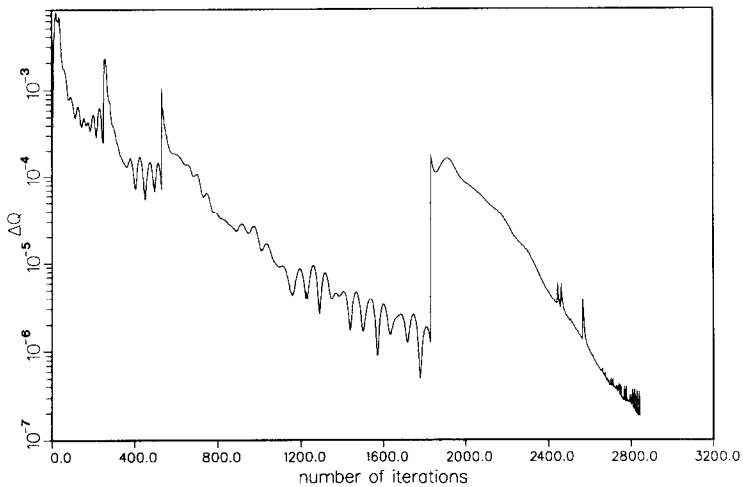

FIG. 3. Variation of ΔQ during the calculation of the flow about the prolate spheroid.

by a considerable jump. However, the largest disturbance appeared when the turbulence model changed at $N = 1830$. It is seen in Fig. 3 that the ΔQ curve presents a discontinuous increase of two orders of magnitude at this point in the convergence history.

Concerning the development in time of the spatial variation of the numerical disturbance field, the present results suggest that when a perturbation is imposed in the solution, large disturbances are generated at those points of the flow (grid) on which the new values imposed are different from the previous ones. During the immediate subsequent cycles of calculation, the disturbances propagate away from the initial regions of disturbance and gradually cover a large volume, which may or may not be equal to the whole calculation domain, depending on the strength of the disturbances. Then the disturbances start to decay, so that gradually the perturbation domain shrinks towards the initial perturbation region and from there towards low value, in the case of a steady flow. The present data has not covered the case of the unsteady flow. However, it seems that in that case numerical disturbances will always be present in the unsteady part of the flow, but not in the whole flow field.

Of great importance for practical applications is the fact that the regions in which the numerical disturbances are large coincide with the regions in which the flow has large gradients. Thus it is easy to anticipate where it will take more time for a numerical solution to converge.

A clear demonstration of the nonuniform generation and decay of the numerical disturbances is given by Fig. 4, in which the history of the development of the numerical disturbance field is given, in the case of the reduction of the value of the numerical dissipation terms. It is seen in Fig. 4 that the disturbances initially appear

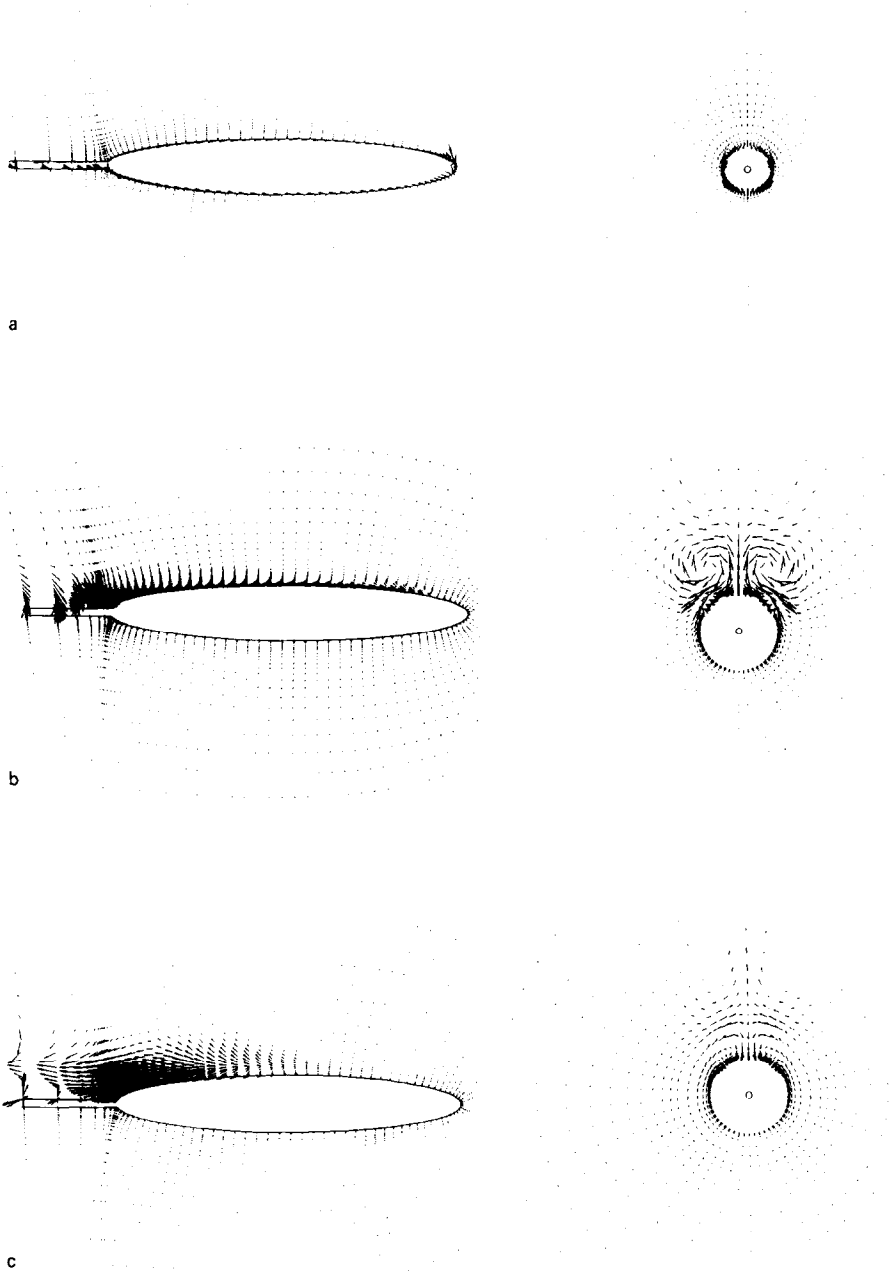

FIG. 4. Prolate spheroid calculations. History of development of the numerical disturbance field, after the solution was disturbed by reducing the numerical dissipation terms.

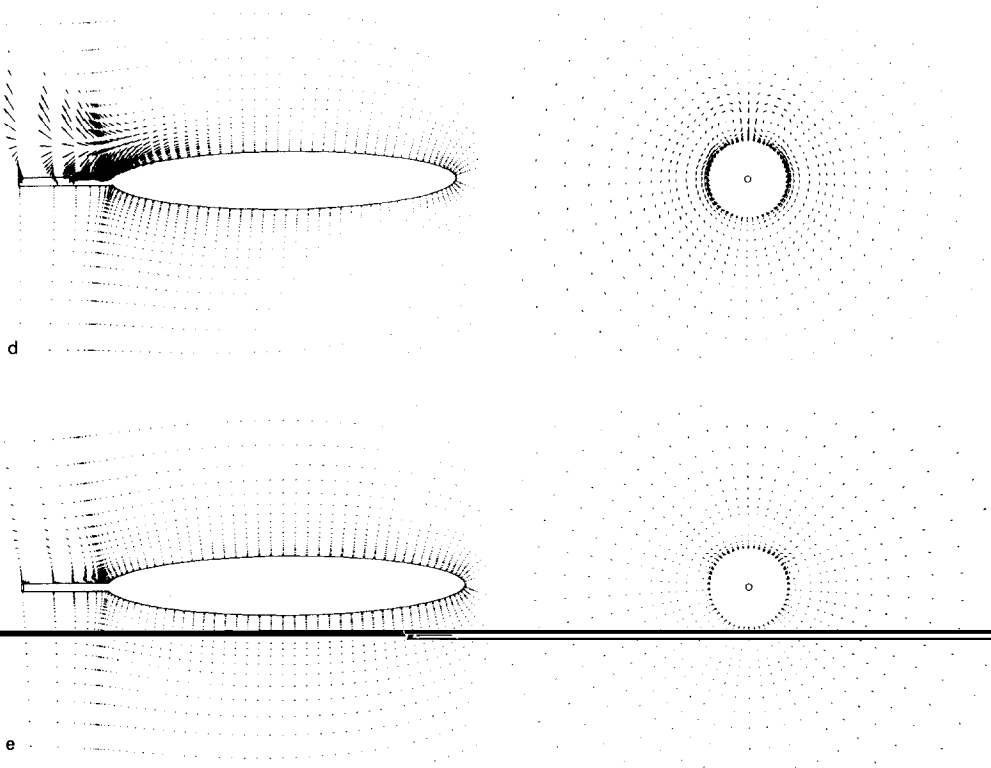

FIGURE 4—*Continued*

near the surface of the body (Fig. 4a). Then they propagate and cover the boundary layer and the vortical separation region at the leeward region (Fig. 4b); in the rest domain, "silence" conditions prevail. Gradually the disturbances die out and uniform conditions of "silence" are established everywhere (Figs. 4c–e).

As additional evidence of the nonuniform convergence of a numerical solution, in Fig. 5 the impact of the modification of the turbulence model on the numerical disturbance field is shown, at the time step $N = 1830$. It has been mentioned in Section 3 that this modification has affected only the separated-flow region and not the attached one. In Fig. 5 the same is seen to happen to the numerical disturbance field. The disturbances appear only in the leeward vortical region, where the crossflow separation exists, propagate outwards to account for the enlargement of the vortices, and gradually decay when equilibrium conditions have been reached. In the windward region, where the flow is attached, the numerical solution is not disturbed at all.

In the case of the impinging jet in the presence of a crossflow, the behaviour of the numerical disturbance field was found to be exactly similar to that of the flow

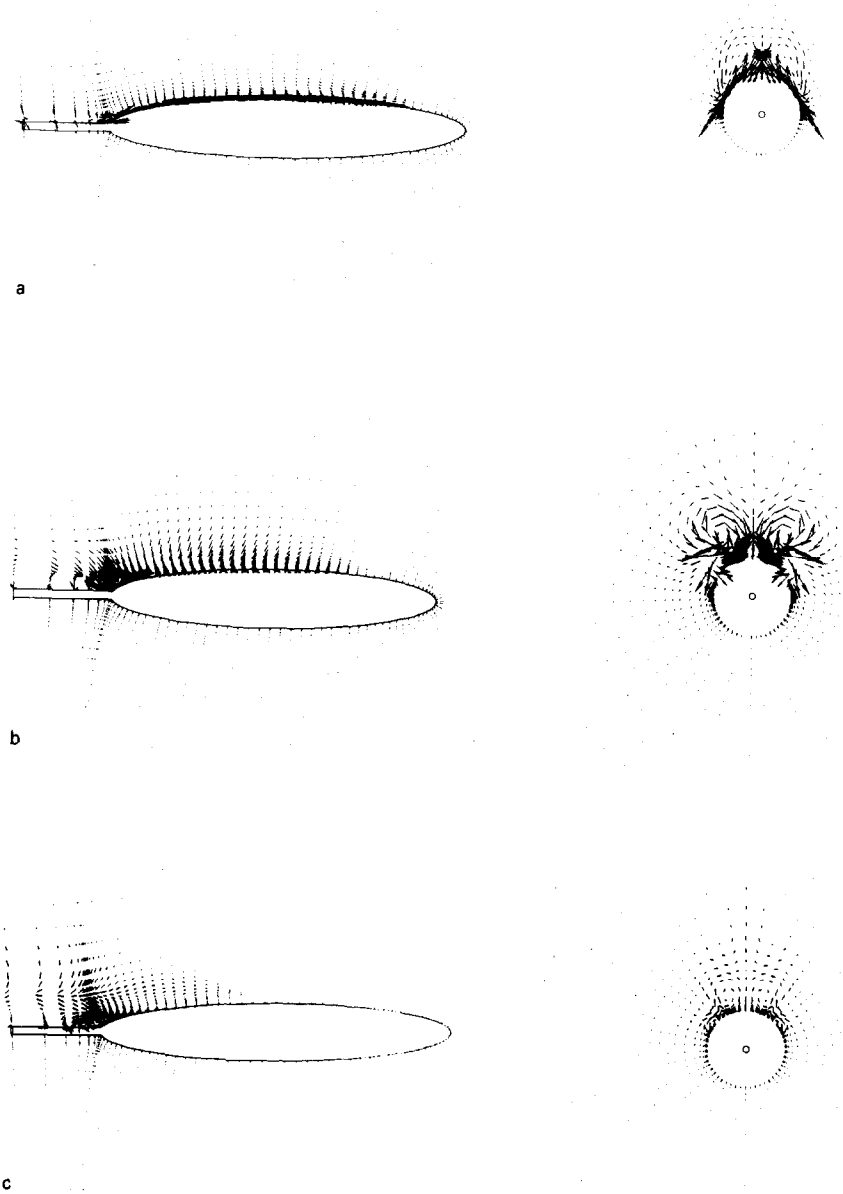

FIG. 5. Prolate spheroid calculations. History of development of the numerical disturbance field, after the solution was disturbed by changing the turbulence model.

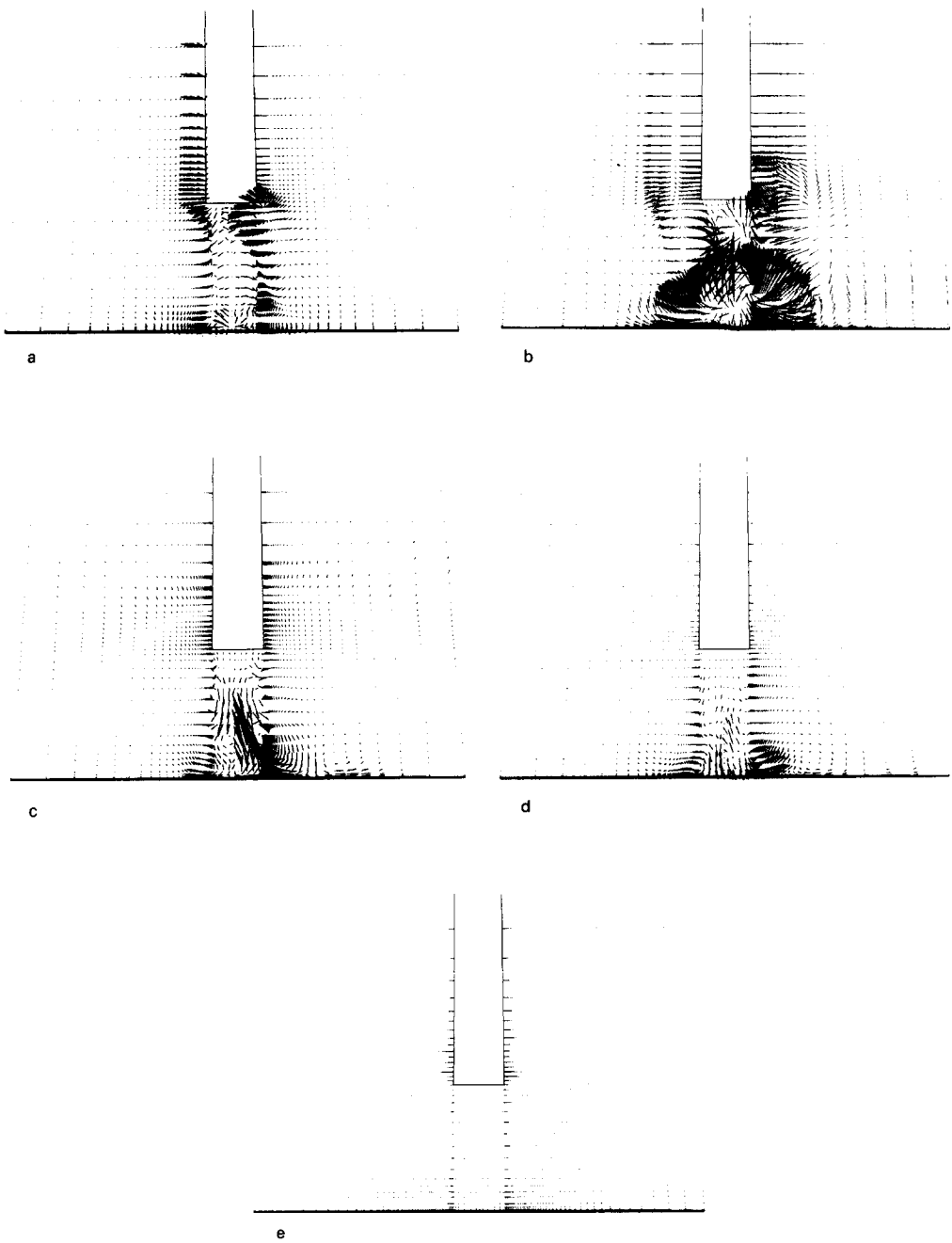

FIG. 6. Jet in crossflow calculations. History of development of the numerical disturbance field, after the solution was disturbed by changing the cross section of the jet from circular to elliptic.

about the prolate spheroid. The evolution of the disturbance field is shown in Fig. 6. As soon as the geometry of the grid is perturbed, by changing the circular nozzle into one of elliptic cross sections large disturbances appear on the upstream face of the nozzle and, mainly, in the region of the jet (Fig. 6a). The disturbances propagate radially but they do not cover the whole calculation domain (Fig. 6b). The equilibrium conditions start to be established initially on the outer layers and gradually reach the jet (Fig. 6c). After 600 steps (Fig. 6d) the disturbance field has been restricted to the vicinity of the jet and of the ground vortex and to the downstream wall flow. From then on, 1100 steps were required for the decay of these localized disturbances (Fig. 6e). The final decay of the disturbances is an indication that the flow is rather steady. Also, Van Dalsem [8] has concluded that the round jet configuration, which he studied, shows only a small unsteadiness. Van Dalsem tried to develop a self-sustained unsteady jet in ground effect, by varying periodically the jet-exit velocity. However, once the forced pulsing was removed the flow quickly returned to a relatively steady state condition.

4.2. *Effect of the Value of the Jacobian*

In the expression of the Navier–Stokes equations in a generalized system of coordinates all the terms are divided by the transformation Jacobian of the system of coordinates. However, the value of the Jacobian within a grid may vary by orders

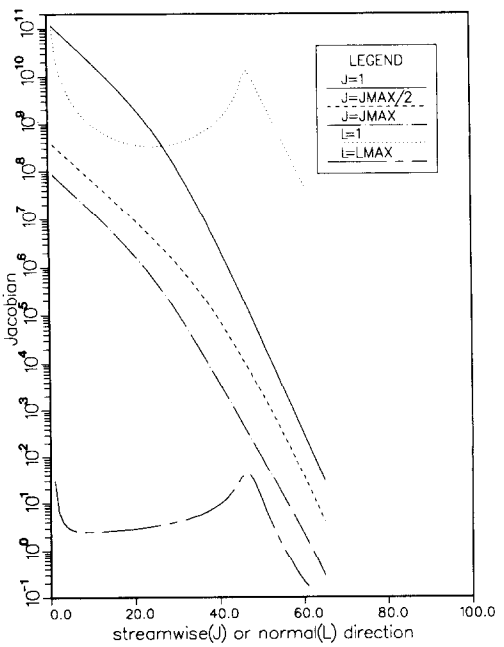

FIG. 7. Prolate spheroid calculations. Variation of the transformation Jacobian of the coordinates, across the grid.

of magnitude. This variation affects the value of the numerical convergence criteria, because the disturbance quantities, on which the criteria are based, have been divided at the various points of the flow field by the variable Jacobian. Thus, the level of the disturbances in regions where the Jacobian has large values will be masked. This undesired effect of the Jacobian will be examined in this section.

The variation of the Jacobian in the crossflow and in the streamwise direction of the prolate spheroid is shown in Fig. 7. In this figure the horizontal coordinate denotes the streamwise (J) or the normal (L) direction to the surface. The scale indicates grid points. The variation of the Jacobian is given in the normal to the surface of the body direction at three streamwise stations: at the origin ($J=1$), in the middle ($J=J_{\max}/2$) and at the end ($J=J_{\max}$) of the body. Also, at two stations, in the parallel to the surface direction: along the wall ($L=1$) and along the $L=L_{\max}$ line. The greatest variation of the Jacobian happens in the normal to the body direction. Thus, on the surface of the ellipsoid the Jacobian may be equal to 10^{10}, depending on the axial position, while at the outer boundaries of the grid it may be even smaller than unity. In the streamwise direction the variation is somewhat smaller, the extreme values vary only three order of magnitude.

In the case of the jet in a cross-flow configuration high values of the Jacobian appear in the vicinity of the jet and near the impingement surface. The value of the Jacobian there is five to seven orders of magnitude greater than in the far field

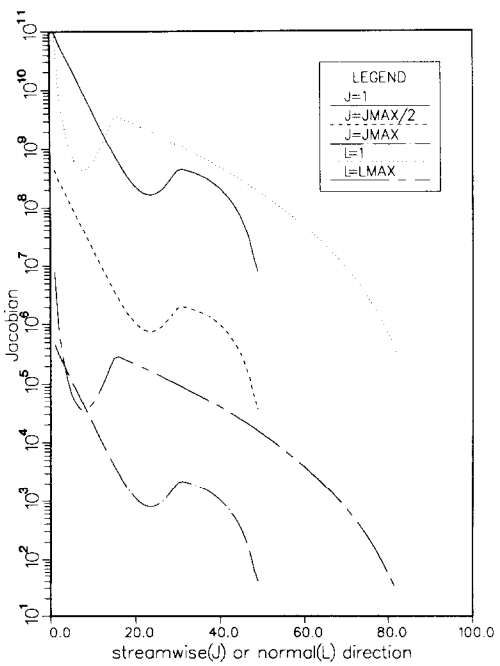

FIG. 8. Jet in crossflow calculations. Variation of the transformation Jacobian of the coordinates, across the grid.

(Fig. 8). However, it is the jet and especially its impingement region where the greater values of the numerical disturbances occur (Fig. 6).

The masking effect of the Jacobian is very clearly shown if the values of the l_2 norm are estimated, during a numerical calculation, with the residual of the Navier–Stokes equations scaled or unscaled by J. The results of this type of calculation are shown in Fig. 9, for the case of the prolate spheroid. The unscaled l_2 norm curve (Fig. 9a) is similar in shape with the ΔQ curve (Fig. 3). All the changes that

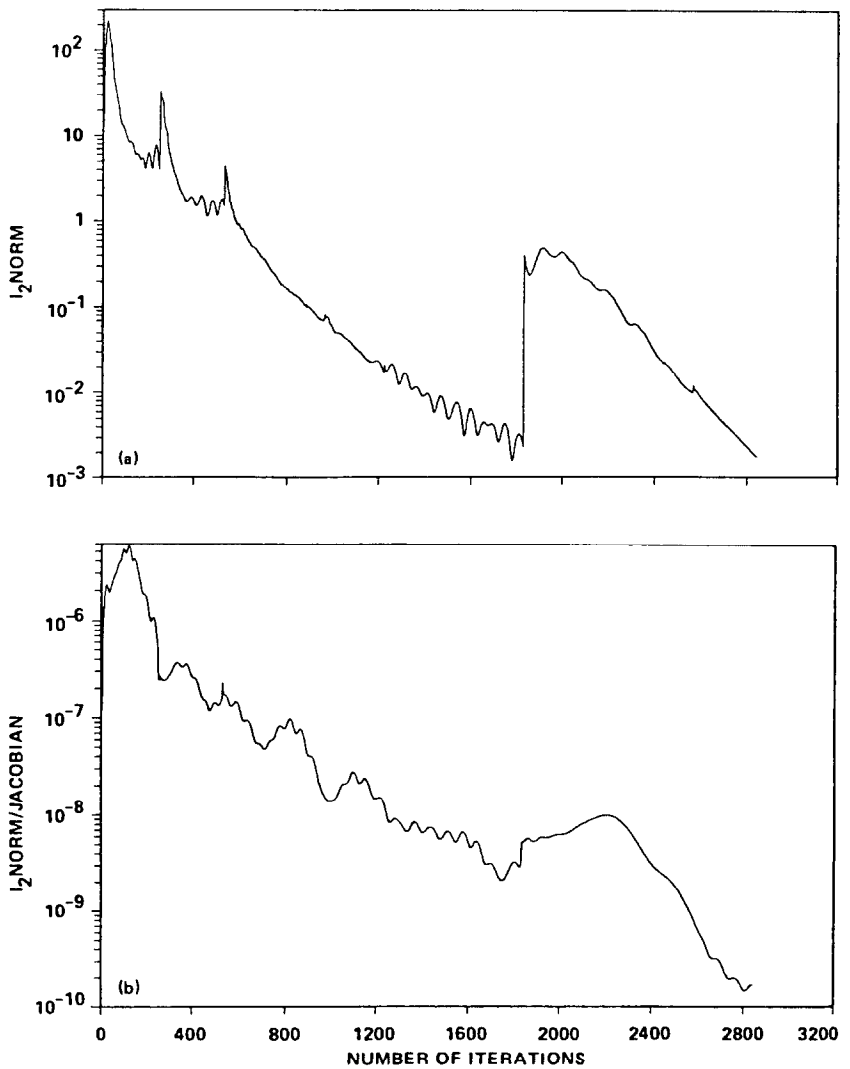

FIG. 9. Prolate spheroid calculations. History of the l_2 norm: (a) unscaled; (b) scaled by the transformation Jacobian.

were applied during the numerical solution are shown in this curve, by discontinuous increases of the disturbance value. On the contrary, it is hard to detect the effect of the changes on the convergence level in the case of the standard l_2 norm curve (Fig. 9b). It is only the change of the turbulence model that somehow is detected, by a small discontinuous change at $N = 1830$, and then by a gradual increase. We are reminded that in this particular application the disturbances start to grow near the surface and then propagate outwards (Section 4.1). In the case of the change of the turbulence model, the outward extent was great because the vortex structure was strongly affected.

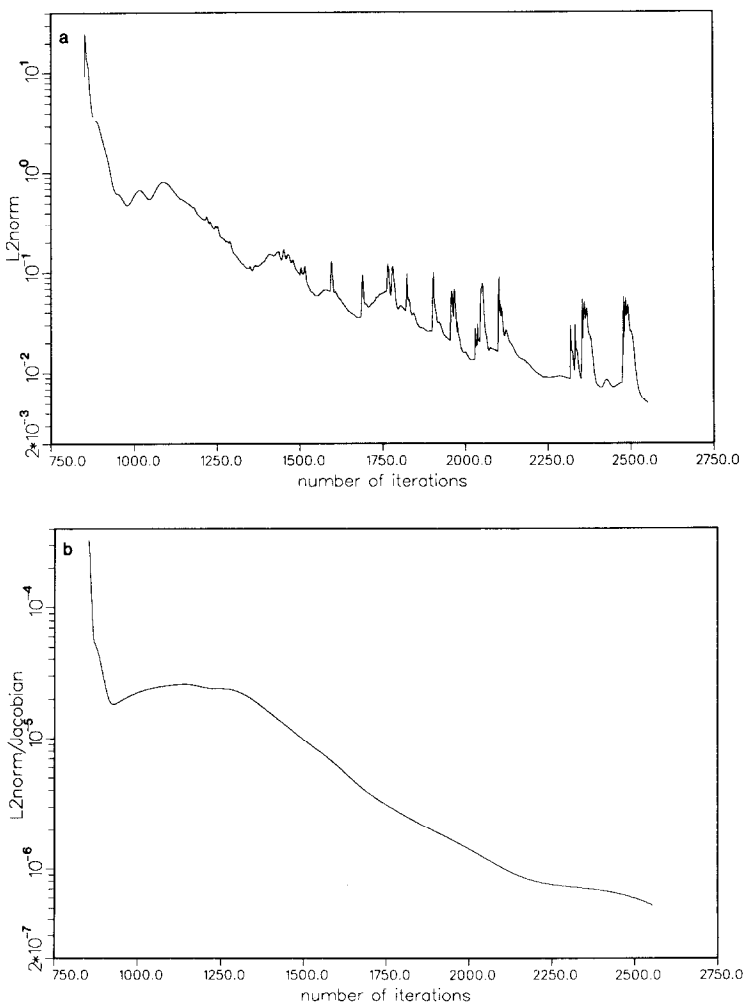

FIG. 10. Jet in crossflow calculations. History of the l_2 norm: (a) unscaled; (b) scaled by the transformation Jacobian.

The same observations apply, also, in the case of the jet in crossflow. The variation of the two l_2 norms is given in Fig. 10. It is seen that while the unscaled l_2 norm curve (Fig. 10a) presents repeated, if not periodic, fluctuations, the standard l_2 norm (Fig. 10b) is very smooth. An examination of the velocity–disturbance plots indicated that these fluctuations correspond to disturbance burstings within the jet at the impingement region near the wall. Most probably these burstings are of numerical nature and do not indicate unsteadiness of the flow. A detailed examination is necessary. It is evident from this example that the standard l_2 norm is not appropriate to detect disturbances near the wall.

The judgment of the state of convergence from the variation of the l_2 norm is more critical in the case of a laminar flow than in the case of a turbulent one, because in a laminar flow the natural dissipation is much smaller. So when the numerical dissipation is reduced at the final stages of a calculation, the overall dissipation is small. Thus, instabilities may develop near the surface of a body, where due to the fineness of the grid the dissipation is very small. A demonstration of the conditions that may develop is provided in Fig. 11, where the disturbance field is shown about the prolate spheroid in the case of a laminar flow. The flow conditions for this calculation were $\alpha = 10°$, $M_\infty = 0.166$, and $\mathrm{Re}_l = 7.7. \times 10^6$. It is seen in Fig. 11 that in a small region near the sting, at the windward side, strong disturbances persist, while in the rest calculation domain the disturbances have decayed. The persistance of these disturbances affects the quality of the predicted flow, locally. If the scaled by the Jacobian l_2 norm is consulted, this local non-convergence is not detected (Fig. 12a). In contradiction, the unscaled l_2 norm, Fig. 12b, clearly indicates that the flow has not converged yet.

A final illustration of the effect of the Jacobian is given in Fig. 13, where the variation of the l_2 norm in the direction normal to the surface of the prolate spheroid is shown, at two positions; one on the windward side of the flow ($\phi = 30°$) and one on the leeward side ($\phi = 150°$). This figure corresponds to Fig. 4b. It is seen, in Fig. 13, that in the case of the unscaled by the Jacobian l_2 norms, their

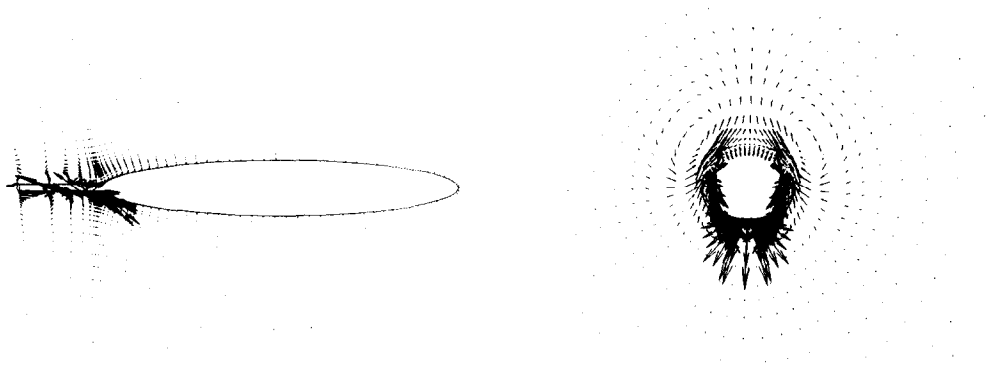

FIG. 11. The numerical disturbance field during the solution of a laminar flow about the prolate spheroid.

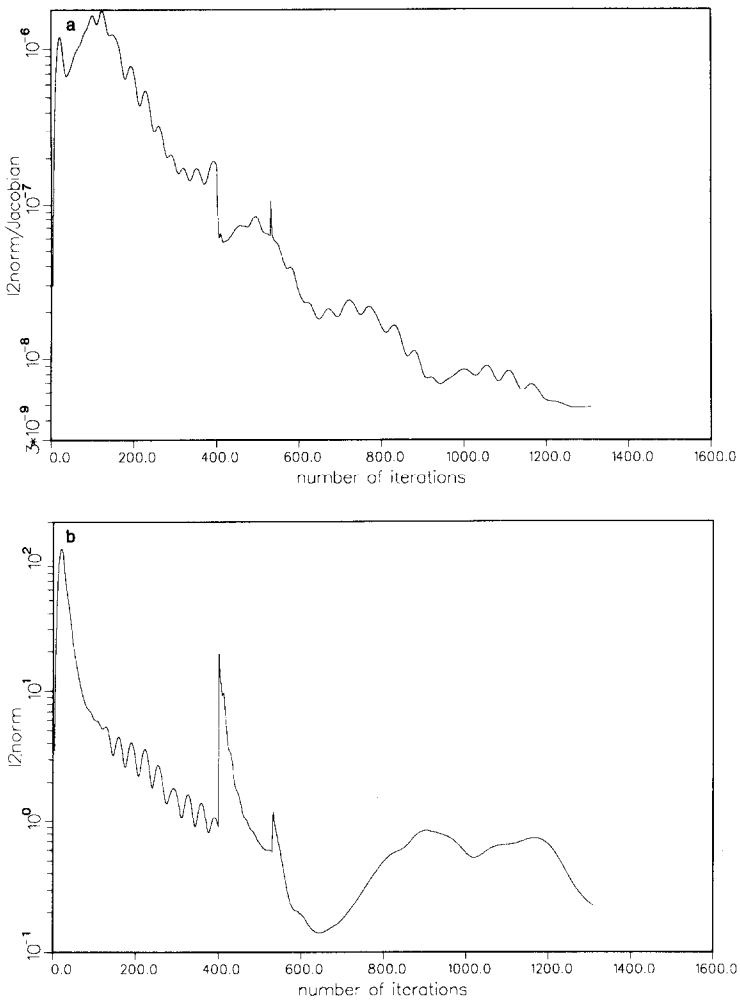

FIG. 12. Laminar-flow about a prolate-spheroid. History of the l_2 norm: (a) scaled; (b) unscaled by the transformation Jacobian.

values are orders of magnitude higher near the surface than in the far field. On the contrary, the scaled l_2 norms have higher values in the far field and not near the surface.

Also, noteworth, in Fig. 13 is the fact that the l_2 norms have an order-of-magnitude higher values in the region of the vortices, on the leeward side, than in the corresponding windward region. This fact is in agreement with the observed variation of the velocity disturbance field shown in Fig. 4b. This justifies the use of the velocity disturbance field for judging the convergence state of a numerical solution.

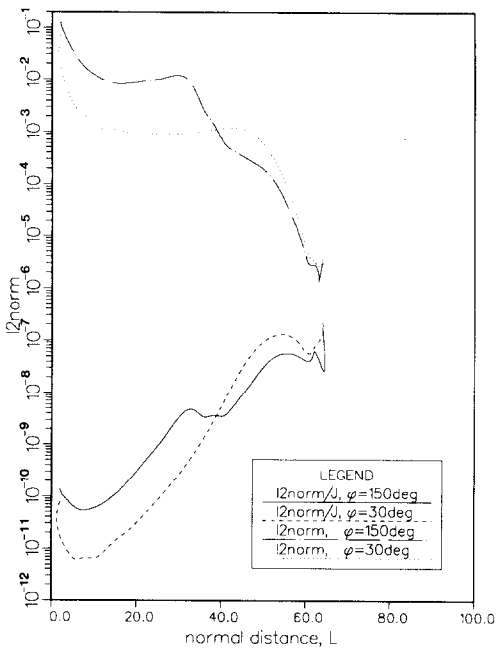

FIG. 13. Prolate-spheroid calculation. Spatial variation of the l_2 norm.

4.3. *Partial-Grid Calculations*

The observed nonuniformity of the numerical perturbation field and the concentration of the disturbances in rather small regions, during most of the calculation time, suggest that for the estimation of a flow field it is worth applying what may be called a partial-grid calculation technique. According to this technique, during a certain number of iteration steps the calculation will be restricted to a region which will be equal to a part of the overall numerical domain. This region will be characterized by the existence of large numerical disturbances, while outside this region the level of disturbances will be very small or zero. In this way a numerical solution will be accelerated, because, although the total number of the iterations will be equal to, or even greater than, the number required for the convergence of the solution by application of the standard technique of the full-grid calculation, the equivalent number of full-grid iterations will be smaller. The technique of local iterations has also been used by Cline [10] in the VNAP codes.

There are various possibilities for the application of the technique of the partial-grid calculation. In case of an unsteady flow, and assuming that an asymptotic steady solution is available, it is necessary to iterate from time to time between the partial-grid solution, which will be aplied to the varying part of the flow and the full-grid calculation, so that the disturbances will be free to propagate.

In the case of a steady flow calculation a reasonable approach is first to reach the

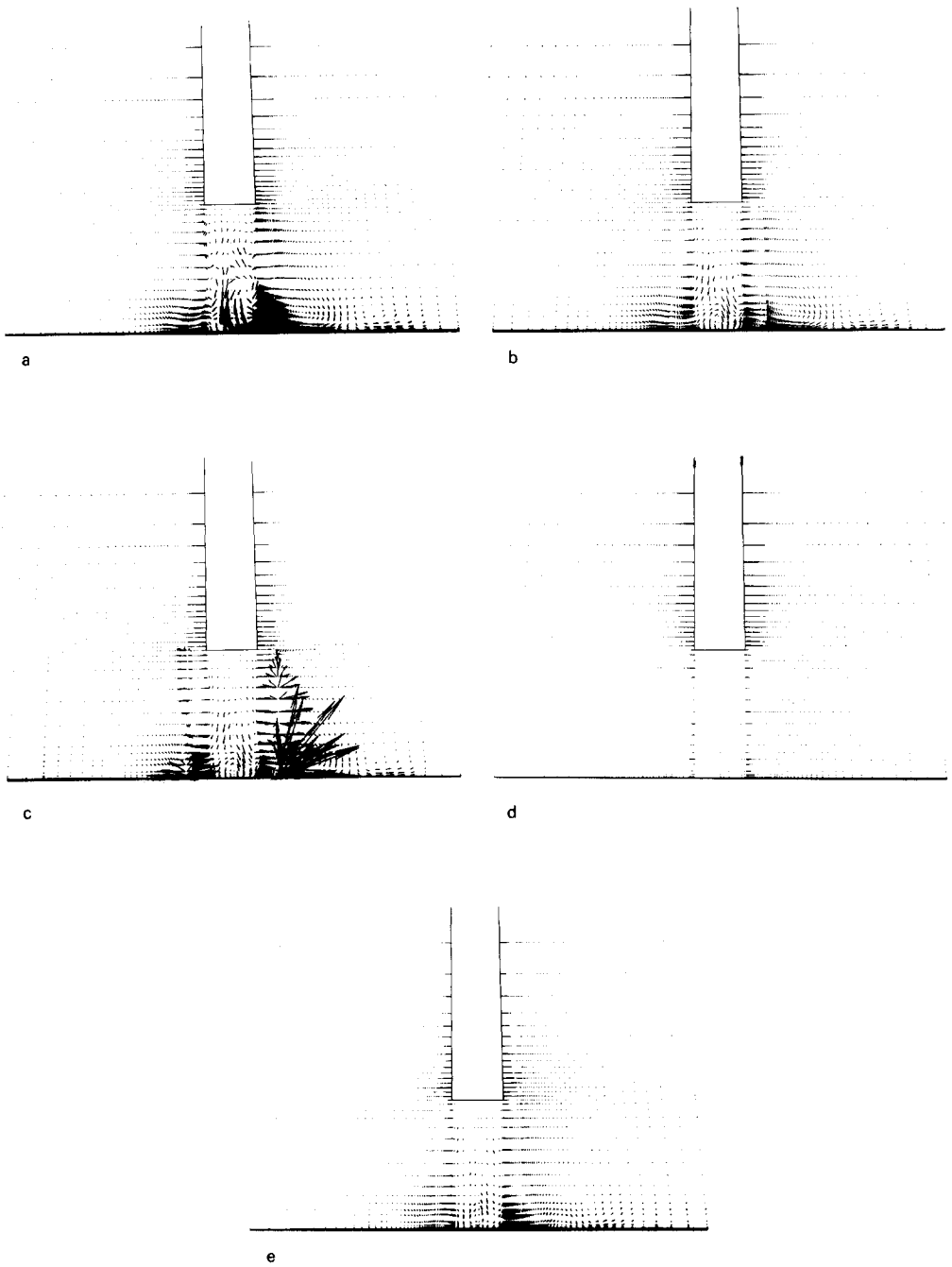

FIG. 14. Partial-grid calculation. History of development of the numerical disturbance field.

full-grid calculation to such a level that the disturbances will be significant only in a small domain; then to apply a partial-grid calculation, until "silence" conditions are established in the disturbance region. After this, the full-grid calculations may be repeated till the flow will be assumed to have converged by means of a mean-value criterion. Alternatively, the full-grid calculations may not be repeated after the partial-grid calculations, if the overall convergence level is considered as being satisfactory.

The technique of the partial-grid calculation was validated by being applied in the case of the impinging jet. The partial-grid calculations started at $N = 500$ of the full-grid solution. Then the partial-grid calculation was applied first to a cylindrical region that starts from the exit of the nozzle, it extends to the ground and encloses the numerically most active part of the jet. The ratio of the partial grid to the full grid was 1:3. After the disturbances were signicantly reduced (300 steps), the radius of the cylindrical region was increased, so that the downstream region of disturbances was enclosed within the calculation domain. The enlarged partial grid was about half of the total grid. The calculation was continued in the enlarged partial grid until the total number of steps became equal to the number required for the full-grid solution to converge, i.e., 1700 steps. The equivalent full-grid number of steps was only 1000. Thus, with this partial-grid calculation about 40% of the computation time was saved.

Some instances of the numerical disturbance field during the partial-grid calculation are shown in Fig. 14; the starting conditions (Fig. 14a), the end of the $\frac{1}{3}$ partial calculation (Fig. 14b), the extension of the calculation to the $\frac{1}{2}$ of the grid (Fig. 14c), and the final conditions (Fig. 14d). If the full-grid calculation procedure was applied, the disturbance field at the equivalent number of steps (consuming the same computation time) would be like the one shown in Fig. 14e. The positive effect of the partial-grid calculation is evident if the equivalent Figs. 14d and 14e are compared. In addition, the final partial-grid results compare well with the final full-grid results (Fig. 6e).

The calculated flow characteristics of the partial-grid solution were the same as those of the full-grid solution. For a qualitative comparison, the development of the mean value of ΔQ is shown in Fig. 15, for both the full-grid and the partial-grid calculation. The mean ΔQ, in the case of the partial-grid calculations is based on the actual domain of calculation. The agreement between the final convergence level of the two calculations and the discontinuous increase of the disturbance value, observed in the partial-grid calculation curve when the grid was extended, are the major points to be noted in Fig. 15, At this point it is clarified that for the estimation of the mean ΔQ during the partial-grid calculation, the upper part of the grid is not considered because the flow there is kept constant and is assumed to have converged sufficiently. If one has to repeat the computation in the whole grid, in a particular application, after applying the partial-grid technique, the flow will be disturbed at the boundaries of the two parts of the grids, but experience has shown that the decay will be very fast, especially if the partial grid is so selected that the disturbances at its boundary are small.

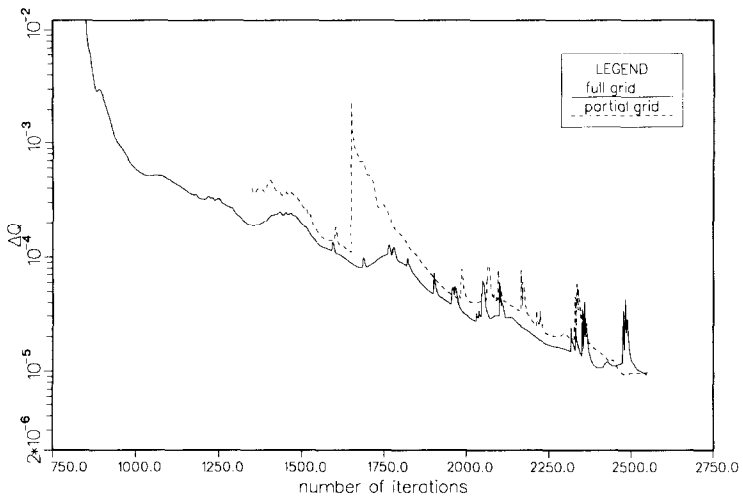

FIG. 15. Variation of ΔQ during the partial-grid calculation

To conclude, the application of the partial-grid calculation technique in the case of the jet in crossflow has demonstrated the potential of this technique in accelerating the convergence of a numerical solution of a flow. In the simple configuration of the jet it was possible to reduce the number of iterations by 40%. In more complicated cases the gain will be higher. For example, if the jet was issued from a wing and not from a cylinder, the grid points which would be included within the jet-disturbance region, where the partial-grid calculation was applied, would be much less than half of the total number of grid points. It is expected that this technique will be beneficial for all flow conditions that include localized complex-flow regions. Also, the study of store separation by application of the multiple mesh scheme [11] is another class of problems, which seems promising for the application of the partial-grid technique. In this scheme a complex configuration is mapped by using a major grid about the main component of the configuration; minor overset meshes are used to map each additional component like a store. It is expected that the disturbances that are generated during the advance in time of the minor meshes (stores) do not cover the whole major grid. So, in such a calculation, it will be sufficient each time to estimate only a part of the flow field about the major component.

5. CONCLUSIONS

In this work, the spatial variation of the numerical disturbances that are generated during a numerical solution of a flow is examined. By considering the generation and decay of the velocity disturbances, it is shown that the disturbance

field is not uniform. More specifically, the decay of the disturbances, or equivalently the convergence of the solution, is fast in regions where the structure of the flow is simple, but it takes a large number of iterations for the disturbances to decay in complex-flow regions, as in separation and vortical areas and in shear flows.

The observed nonuniformity of the numerical disturbances makes the reduction of the calculation time possible by application of the partial-grid calculation technique, in which a part of the calculation procedure is applied in selective subregions, where the velocity disturbances are large, and not within the whole grid. In the particular case of the jet in ground effect that the partial-grid technique was tested, a 40% reduction of the number of iterations was obtained. It is expected that this technique will prove beneficial in large-scale calculations, such as the flow about complete aircraft configurations at high angles of attack, the study of vortices generated on the tips of a helicopter rotor, and the shock-boundary layer interaction observed on the upper surface of a wing.

The partial-grid calculation technique may be viewed as belonging to the same class of acceleration methods with the multigrid method, i.e., by controlling the grid. However, it is noted that their principles and purpose are quite different. While the partial-grid technique is based on the locally non-uniform decay of the numerical disturbances, the multigrid method essentially deals with the stiffness of the system of the difference equations; its purpose is the damping of the high-frequency waves by employing a sequence of successively coarser grids in addition to the selected fine grid. Actually the two methods may be combined in the same calculation scheme.

A secondary issue that has been addressed in the present paper is the effect of the Jacobian of the coordinate transformation on the value of the mean-value criteria, such as the l_2 norm, if the Navier–Stokes equations are written in a generalized coordinate system. In this case all the terms of the equations are divided by the transformation Jacobian. In practice, when the equations are solved numerically, the scaling of the terms by the Jacobian is used during the whole procedure. The solution of the flow, i.e., the Q-vectors, are unscaled at the end of the computation. Thus, when the quantities, on which the calculation of the norms or of the mean ΔQ is based, are evaluated during an iteration, they include the effect of the Jacobian. Consequently, their value appears to be infinitesimally small in regions in which the grid is fine, such as near solid boundaries, because in these regions the Jacobian has very large values. Actually, they reflect changes that happen at the outer boundaries of the computation domain, where the Jacobian approaches unity and not in the whole flow field. This situation is corrected if the quantities on which the mean-value criteria are based are unscaled by the Jacobian, before convergence tests are conducted, at each time step. Of course, unscaling is not the only remedy. Many investigators employ relative error tests, basically to handle scaling problems in general, independent of whether they arise from geometry.

In this paper the velocity disturbance field was used for judging the convergence state of a numerical solution. This type of plot proved very useful. Details that otherwise would not be detected, like the existence of small instability regions near

the surface of a body, were easily identified. The use of the velocity disturbance field is highly recommended in large-scale computing, where a calculation requires many computer hours and it is not done at once.

ACKNOWLEDGMENTS

The author would like to thank Dr. Terry L. Holst and Dr. Thomas H. Pulliam, of NASA/Ames Research Center, for their constructive suggestions for the improvement of the content of the paper. The valuable suggestions of the reviewers are also acknowledged.

REFERENCES

1. S. X. YING, J. L. STEGER, L. B. SCHIFF, AND D. BAGANOFF, AIAA Paper 86-2179, Willamsburg, VA, 1986 (unpublished).
2. B. S. BALWIN AND H. LOMAX, AIAA Paper 78-257, Huntsville, AL, 1978 (unpublished).
3. J. L. STEGER, *AIAA J.* **16**, 679 (1978).
4. T. H. PULLIAM AND J. L. STEGER, *AIAA J.* **18**, 159 (1980).
5. P. G. BUNING, Ph.D. thesis, Stanford University, 1983 (unpublished).
6. T. H. PULLIAM, *Appl. Numer. Math.* **2**, 441 (1986).
7. D. DEGANI AND L. B. SCHIFF, *J. Comput. Phys.* **66**, 173 (1986).
8. W. R. VAN DALSEM, AIAA Paper 87-2279, Monterey, CA, 1987 (unpublished).
9. W. R. VAN DALSEM, A. G. PANARAS, AND J. L. STEGER, SAE Paper 87-2344, Santa Clara, CA, 1987 (unpublished).
10. M. C. CLINE, Los Alamos National Laboratory Report LA-8872, 1981 (unpublished).
11. F. C. DOUGHERTY, J. A. BENEK, AND J. L. STEGER, NASA Technical Memorandum 88193, 1983 (unpublished).